

# A Novel Multi-Resolution Wavelet Transform for Online Power Grid Waveform Classification

Shiyuan Wang, *Student Member, IEEE*, Payman Dehghanian, *Member, IEEE*, and Yingzhong Gu, *Member, IEEE*

**Abstract**—Power grid operation continuously undergoes several state transitions over time primarily driven by the internal (e.g., equipment failures) and external (e.g., weather-driven faults, and/or loading and generation variations) uncertainties. This engenders an observation of different types of waveforms at the measurement points (substations) in power systems captured by the phasor measurement units (PMUs) and intelligent electronic devices (IEDs) embedded with PMU functionality, e.g., digital relays and fault recorders. The PMU should be, hence, equipped with either one synchrophasor estimation algorithm (SEA) that is accurate and robust to many different types of signals that may be inputted at different time intervals across the network, or should adaptively select the promising SEA, among an embedded suite of algorithms, that can best capture an unfolding event. This paper suggests a novel wavelet transform, the pseudo continuous quadrature wavelet transform (PCQ-WT) algorithm, for online power grid events and waveform classification, enabling design or selection of the right SEA when exposed to different events, thus resulting in a more accurate synchrophasor estimation and heightened situational awareness spatially and temporally. Test signals generated from different prevailing events in the IEEE 34-bus test system are applied to verify the robust performance of the proposed classification approach.

**Index Terms**—Phasor Measurement Unit (PMU); Synchrophasor Estimation Algorithm (SEA); Waveform classification; Wavelet transform.

## I. INTRODUCTION

The wide deployment of the synchrophasor technology in recent years has revolutionized the traditional measurement setting in power grids into a new paradigm with high-resolution measurements via which an enhanced system-wide situational awareness is achieved. Synchrophasor measurements, captured across the network via phasor measurement units (PMUs), have transformed many applications, e.g., power system model validation, state-estimation, dynamic stability, real-time monitoring, protection, and control of the grid, and post-event analysis, among many others [1]–[6]. IEEE standard C37.118.1-2011 [7], has defined the expected PMU outputs—i.e., magnitude, phase angle, frequency, and rate of change of frequency (ROCOF)—and their corresponding desirable accuracy which have been deemed to be sufficient to capture the power grid steady-state and dynamic behaviour when transitioning through different operating states over time [8]. Depending on the type of the PMU, whether it is an M-Class with high-accurate measurement requirements for

operation applications (e.g., state estimation) or P-Class with high-speed low-latency requirements for real-time protection and control applications (e.g., fault detection and location), several algorithms have been proposed in the literature.

The synchrophasor estimation algorithms (SEA) are primarily driven by mathematical approximations, e.g., Discrete Fourier Transform (DFT) [9], Kalman filtering [10], adaptive filtering [11], Newton approximations [12], zero-crossing techniques [13], phase locked loops (PLL) [14], and many other variations of these algorithms. In most cases, and irrespective of the focused end-use applications, marketplace PMUs are typically furnished with one of the above SEA tools, each unleashing distinctive advantages and limitations, solely valid to one or a few certain applications. Laboratory tests and field observations have revealed how inefficient the PMU measurements could be if this "one-size-fits-all" approach using only one SEA is applied in the face of different operating states in the system to capture both static and dynamic features and peculiarities [15]–[17]. The growing demand for high-speed low-latency, and yet absolutely accurate, measurements across the grid calls for a more efficient mechanism that can selectively adapt to various evolving operating states by opting the right SEA at the right time.

Recent research efforts have been directed toward dynamic SEA through time-domain signal processing techniques. Such algorithms, although revealing a promising performance under slow-transient conditions (e.g., modulation) [18], quite fail in the presence of abrupt changes in the waveforms (e.g., faults) [17]. In response, some references have proposed one single PMU equipped with a suite of multiple algorithms inside, so called P/M-Class PMU, which is deemed to be effective in response to various prevailing conditions in the grid. Such an approach requires an advanced feature extraction and waveform classification mechanism that can accurately capture and harness the signal peculiarities corresponding to different events and unfolding conditions, and subsequently a selection mechanism to choose the best SEA within the PMU depending on the focused application and the measurement performance requirements over time.

Waveforms in power grid typically reveal a certain pattern with specific features and peculiarities driven by the system operating conditions. For instance, phasor magnitudes and phase angles go through step changes during faults [19] and the measurements can be noisy [10]. Unbalanced load, voltage surge or sag, harmonics, and frequency drift are also common phenomena in electrical power networks [20]–[22]. Many research efforts can be found in the literature on pattern recognition and waveform classification for power quality and

S. Wang and P. Dehghanian are with the Department of Electrical and Computer Engineering, The George Washington University, Washington, DC 20052 USA (e-mail: shiyuan1225@gwu.edu; payman@gwu.edu).

Y. Gu is with the GEIRI North America, San Jose, CA 95134 USA (email: yingzhong.gu@geirina.net).

fault analysis [23]–[28]. To the best of the authors’ knowledge, however, only a few have been focused on waveform classification for PMU applications and online event detection [3], [18]. In this paper, a pseudo continuous quadrature wavelet transform (PCQ-WT) is proposed dedicated to feature extraction and waveform classification of PMU input signals coming from the power grid. The proposed PCQ-WT ensures a fast feature extraction well within the standard requirements, wide range of frequency coverage through a reduced number of scaling factors, and distinguished performance during different events. The performance of the proposed PCQ-WT approach has been tested and verified under various spatially and temporally categorical conditions in a test system.

The rest of the paper is structured as follows. Section II presents the problem statement on the waveform feature extraction and classification through various signal transforms such as continuous wavelet transform (CWT) and the pseudo-continuous wavelet transform (PCWT). Section III introduces the 1-D PCWT, and accordingly the novel PCQ-WT, with the corresponding formulations. Numerical case studies and performance evaluation results are reported in Section IV, followed by the conclusions in Section V.

## II. WAVEFORM FEATURE EXTRACTION AND CLASSIFICATION

Short-time Fourier transform (STFT) and continuous wavelet transform (CWT) are two most commonly used multi-resolution waveform classification techniques in many engineering disciplines [29], [30]. During the feature extraction process, both transforms require a window (buffer) of samples and therefore, a latency effect indeed exists. Selection of a proper window size could minimize the latency effect, but at the cost of trading off the frequency resolution. Note that the frequency is actually estimated from the synchrophasors. With no additional latency, the classification will enable an adaptive selection of the SEA within a PMU, and hence, the instantaneous synchrophasor measurement would be theoretically ensured.

The STFT can extract the waveform frequency spectrum through the Fourier transform on a fixed sampling window. Similarly, the CWT is achieved by assessing the correlations between the signal of interest and the mother wavelet with a continuous frequency scale factor. Figure 1 illustrates the feature extraction results from both STFT (a and b) and CWT (c and d). While it can be clearly observed that the frequency accuracy of the STFT outperforms that of the CWT, CWT stands out for fast feature extraction and event detection. Therefore, CWT is focused in this paper as the main waveform classification approach for online synchrophasor-based applications.

### A. Basic Waveform Representation

First, we define the basic representation of signals in the power grid when transiting to different operating states. Since PMU devices can be installed at any desired location (i.e., substation) in the network, three-phase or single-phase voltage and current signals can be captured. Ideally, the input

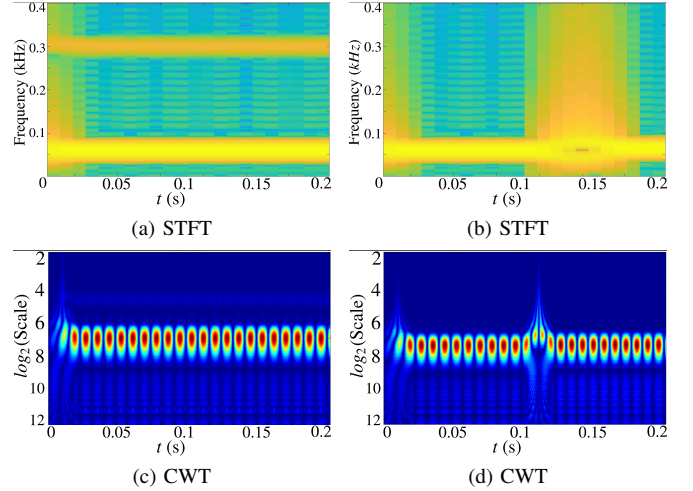


Fig. 1. Comparison of the STFT and Morlet CWT during: (a),(c) the steady-state 60Hz and the 5<sup>th</sup> harmonic pollution; (b),(d) 5Hz frequency ramp.

waveforms to the PMUs are time-domain sinusoidal signals, as represented in (1).

$$x(t) = A(t) \cos \left( 2\pi \int_0^t f(\tau) d\tau + \phi(t) \right) \quad (1)$$

where  $A(t)$ ,  $f(\tau)$ ,  $\phi(t)$  are, respectively, the instantaneous magnitude, frequency, and phase angles. Since the input waveform is captured from a one-phase electrical signal, the waveform  $x(t)$  is a one-dimension (1-D) signal.

### B. CWT and Pseudo-CWT (PCWT)

Wavelet transform is centered on the cross-correlation computations between the signal of interest,  $x(t)$  in this paper, and a designated wavelet, defined as follows:

$$X_\omega(a, b) = \frac{1}{\sqrt{|a|}} \int_{-\infty}^{\infty} x(t) \overline{\Psi} \left( \frac{t-b}{a} \right) dt \quad (2)$$

where  $\Psi(t)$  is the mother wavelet function and  $\overline{\Psi}(t)$  is the complex conjugate of  $\Psi(t)$ ;  $a$  and  $b$  are, respectively, the scaling factor and the time shift; and  $\Psi(\frac{t-b}{a})$  is one of the "daughter wavelets" of  $\Psi(t)$  [31]. With different selections of  $a$  and  $b$ , a set of daughter wavelets is then defined, characterizing the correlations between the input signal  $x(t)$  and the daughter wavelets. When proper intervals for the *continuous* scaling factor along with the time shift are selected, a continuous-wavelet transform (CWT) is achieved [32].

Real-time signal amplitude quantization and sampling are nowadays very well developed and widely applied in different disciplines. The continuous-time to discrete-time (C2D) conversion will, however, sabotage the continuity of the real-time signal. Mathematically, the daughter wavelets' length or the so called the wavelet window size is limited. And at the same time, the scaling factor is finite due to the processing capacity limitations of the computing hardware. Furthermore, the scaling factors are obviously not continuous parameters in practical settings of digital signal processing (DSP). More importantly, shorter window size and less scaling factors will reduce the feature extraction latency and the computational

burden; however, the performance of the discrete wavelet transform must not be compromised comparing to the continuous time application. For all these reasons, the actual behavior of the CWT is pseudo-continuous, even with less discrete scaling factors used, but the performance needs to be close to the discrete implementation of the CWT. Here, the pseudo-CWT (PCWT) is defined as

$$X_\omega[a, b] = \frac{1}{\sqrt{|a|}} \sum_{n=0}^{W-1} x[n] \bar{\Psi}\left[\frac{nT_s - b}{a}\right] \quad (3)$$

where  $T_s$  is the sampling interval;  $W$  is the window length. In contrast with the discrete wavelet transform (DWT)'s dyadic increase of the scaling factor, the scaling factor increment in the PCWT is preset to be linear, but still plotted in a reversed-dyadic format. The central frequency of the daughter wavelet has the following relationship with the scaling factor:

$$f = F_c/a \quad (4)$$

where  $F_c$  is the central frequency of the mother wavelet [32]. Hence, as  $a$  increases, the position of the WT output decreases in the frequency domain. In order to match the frequency positive increment along the Y-axis, all scales in WT plots illustrate a descending trend in all figures.

### C. PCWT's Feature Extraction Mechanism

The proposed waveform classification approach is centered on the extraction of distinct features in the input power waveform. To reveal the signal composition at any given operating condition, the "frequency spectrum" or the PCWT output must be featured with a redundant range in order to provide sufficient pattern information. Therefore, in addition to the fundamental frequency, a proper selection of the central frequency and a sufficient length of the scaling factor are requisite. Strict mathematical derivations are pursued to find the central frequency  $F_c$  and the scaling factors. To serve the research focus on the feature extraction wavelet,  $F_c$  is chosen arbitrarily from a frequency range higher than the fundamental frequency, scaled down by  $a$ .

There are multiple mother wavelet families, and consequently, different mother wavelets will yield distinct results. Figure 2 demonstrates the performance of six mother wavelet families on a steady-state 60Hz sinusoidal signal. Before time  $t = 0$ , all waveform data are set to be zero. Figure. 2(a) and (d) reveal a relatively higher concentration of the correlation strength by applying the Morlet and 4<sup>th</sup>-order Gaussian wavelets, respectively. In contrast, Figure. 2(b) has shown the widest spectrum, indicating a stronger capability of the Haar wavelet in capturing frequency variations within a range of interest—This is, however, not suitable for feature extraction in steady-state conditions. All the frequency features captured in Fig. 2 are plotted over time  $t$ .

In order to accurately follow the PCWT procedure, the requisite buffer to perform the operation in (3) needs to wait a time interval to be filled. A moving window approach is pursued in this paper, application demonstration of which is presented in Fig. 3. The distortions from time zero in all test cases presented in Fig. 2 can be explained by the *edge effect*

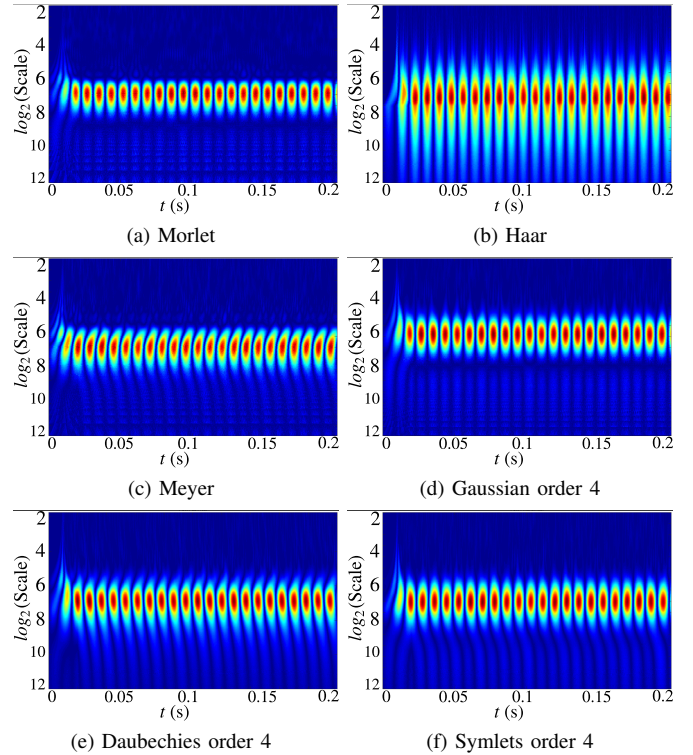


Fig. 2. Output comparison of six different mother wavelet families on a 60Hz sinusoidal waveform.

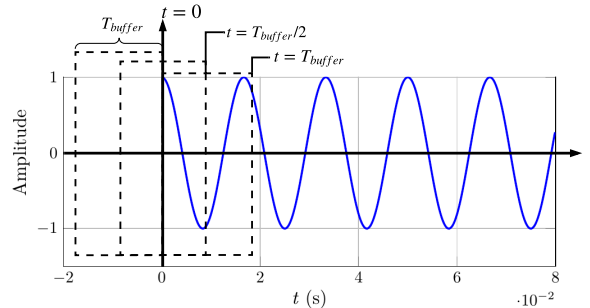


Fig. 3. Demonstration of the moving window approach in the PCWT applied to the input waveform.

[33]. In order to compensate for the edge effect, the window size can be chosen narrower, resulting in a smaller buffer size that takes less time to be filled. This solution, however, decreases the PCWT output resolution.

### III. THE PROPOSED WAVELETS BASED ON THE PCWT

The proposed wavelets essentially perform a multi-resolution correlation calculations as described in the previous Section. From Fig. 2, one can see that the wavelet transform—and PCWT—can generally provide the frequency information; we, however, focus on the feature extraction of the power waveforms. Such information can be then leveraged and inputted to a selected synchrophasor estimation algorithm for accurate measurements.

### A. Proposed 1-D PCWT for Feature Extraction

Inspired by the band limited characteristic of the Shannon wavelet, which can be applied to power network signals with limited range of fundamental frequency, this paper proposes a narrow-bandwidth wavelet algorithm. Note that the term "feature" is here referred to a unique behaviour in a particular event or phenomenon in dynamic power grids—e.g., frequency and amplitude patterns. Analytic expression of the Shannon wavelet is as follows [34], [35]:

$$\Psi^{(Shannon)}(t) = \underbrace{\gamma_b^{\frac{1}{2}} \text{sinc}(\pi\gamma_b t)}_{\text{Vanishing Component}} \cdot \underbrace{\cos(2\pi F_c t)}_{\text{Periodic Component}} \quad (5)$$

where  $\gamma_b$  is the desired bandwidth. As can be seen, this wavelet expression is composed of a periodic and a vanishing component in time. The wavelet is always featured with a finite length in the time domain. As the period of the fundamental signal and harmonics are those components of interest in power grids, the periodic component is much preferred in the mother wavelet. Furthermore, when the time deviates from the center, the amplitude vanishes faster in time. The general format of the proposed mother wavelet ( $a = 1$ ) is

$$\Psi^{(P)}(t) = \underbrace{\frac{\sqrt{2}}{1 + \cosh(\pi F_c t)}}_{\text{Vanishing Component}} \cdot \underbrace{\cos(2\pi F_c t)}_{\text{Periodic Component}} \quad (6)$$

The Periodic Component is still the same as that in the Shannon wavelet; the proposed mother wavelet uses hyperbolic function to drive the amplitude of daughter wavelet fading faster at high frequency and slower at lower frequency; thus, the fundamental component reveals more details shown in the scaleogram. Before applying (6) into (2) to perform the WT, the central frequency  $F_C$  should satisfy the condition in (7).

$$\frac{F_c}{\max(a)} < f_0 < F_c \quad (7)$$

where  $f_0$  is the frequency of the signal of interest. The proposed CWT algorithm applied to a sinusoidal waveform assumes that the wavelet's center is fixed at  $t = 0$  on the horizontal time axis, i.e  $b = 0$ , and the target sinusoidal waveform is moving towards left hand side in Fig. 3. For simplicity, we keep  $f_0(t)$  constant,  $A(t) = 1$ , and  $\phi(t) = 0$ ,

$$\begin{aligned} X_{\omega|a,b}^{(P)} &= \frac{1}{\sqrt{2a}} \sum_{n=0}^{W/2} \frac{\cos[2\pi(f_0 + \frac{F_c}{a})T_s n]}{(e^{\pi \frac{F_c}{2a} T_s n} + e^{-\pi \frac{F_c}{2a} T_s n})^2 / 4} + \frac{1}{\sqrt{2a}} \sum_{n=0}^{W/2} \frac{\cos[2\pi(f_0 - \frac{F_c}{a})T_s n]}{(e^{\pi \frac{F_c}{2a} T_s n} + e^{-\pi \frac{F_c}{2a} T_s n})^2 / 4} \\ &= \frac{1}{\sqrt{2a}} \sum_{n=0}^{W/2} \frac{\cos[2\pi(f_0 + \frac{F_c}{a})T_s n]}{\cosh^2(\pi \frac{F_c}{2a} T_s n)} + \frac{1}{\sqrt{2a}} \sum_{n=0}^{W/2} \frac{\cos[2\pi(f_0 - \frac{F_c}{a})T_s n]}{\cosh^2(\pi \frac{F_c}{2a} T_s n)} \end{aligned} \quad (9)$$

the CWT can be then presented as follows.

$$\begin{aligned} X_{\omega|a,b=0}^{(P)} &= \frac{1}{\sqrt{a}} \int_{-\infty}^{\infty} x(t) \overline{\Psi}^{(P)}\left(\frac{t}{a}\right) dt \\ &= \frac{\sqrt{2}}{\sqrt{a}} \int_{-\infty}^{\infty} \frac{\cos(2\pi f_0 t) \cos(\frac{2\pi F_c t}{a})}{1 + \cosh(\pi \frac{F_c t}{a})} dt \\ &= \frac{\sqrt{2}}{\sqrt{a}} \int_0^{\infty} \frac{\cos[2\pi(f_0 + \frac{F_c}{a})t] + \cos[2\pi(f_0 - \frac{F_c}{a})t]}{1 + (e^{\pi \frac{F_c t}{a}} + e^{-\pi \frac{F_c t}{a}})/2} dt \\ &= \frac{\sqrt{2}}{\sqrt{a}} \int_0^{\infty} \frac{\cos[2\pi(f_0 + \frac{F_c}{a})t] + \cos[2\pi(f_0 - \frac{F_c}{a})t]}{(e^{\pi \frac{F_c t}{2a}} + e^{-\pi \frac{F_c t}{2a}})^2 / 2} dt \end{aligned} \quad (8)$$

Converting the continuous-time structure of (8) to a discrete-time form, the continuous scaling factors are also converted to discrete with reduced number of elements—i.e., pseudo-continuous—and the proposed PCWT algorithm for waveform feature extraction is achieved, as presented in (9). The resulting set of scaling factors can be eventually applied to the proposed mother wavelet to form a wavelet bank. Such a wavelet bank can be loaded into digital computing devices to perform the proposed PCWT. In order to achieve a desired performance of the proposed PCWT algorithm, the window size  $W$  must have sufficient length. Analytically, the first summation will tend to be very small as the periodic component of the signal has a frequency of  $|f_0 + \frac{F_c}{a}| \gg 0$ , resulting in small correlation coefficients. Thus, the first summation plays less of an impact on the energy "spectrum" than the  $|f_0 - \frac{F_c}{a}|$ , since,

$$|f_0 + \frac{F_c}{a}| > |f_0 - \frac{F_c}{a}| \geq 0 \quad (10)$$

when  $f_0 = F_c/a$ , the daughter wavelet will result in the highest correlation coefficients with respect to the waveform dominating component. This will yield a maximum value of the second summation function. Furthermore, the vanishing component will confine the second summation within a reasonable upper limit, thus the computing memory would not overflow. The proposed mother wavelet and its decomposition is illustrated in Fig. 4(a) while its daughter wavelets are demonstrated in Fig. 4(b),(c).

### B. Transformation of 1-D PCWT to the PCQ-WT

In three-phase power networks, the Clarke transform is widely applied to convert the time-domain components of a three-phase signal in an ABC-reference frame to components in a stationary  $\alpha\beta 0$ -frame [36]. The time-domain  $\alpha\beta$  compo-

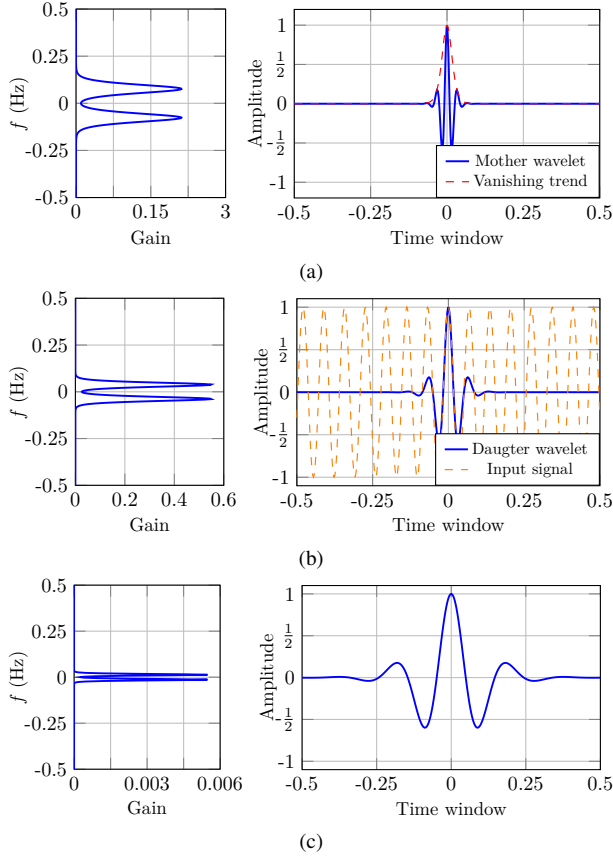


Fig. 4. Proposed wavelets for waveform online feature extraction; left figure: spectrum; right figure: wavelet. (a) mother wavelet, (b) daughter wavelet with scaling factor 11, (c) daughter wavelet with scaling factor 26.

nents will be utilized to generate a complex time signal as presented in (11) and (12).

$$x_{\alpha\beta}(t) = x_{\alpha}(t) + jx_{\beta}(t) \quad (11)$$

$$\begin{bmatrix} x_{\alpha}(t) \\ x_{\beta}(t) \end{bmatrix} = \begin{bmatrix} \frac{2}{3} & -\frac{1}{3} & -\frac{1}{3} \\ 0 & \frac{\sqrt{3}}{3} & -\frac{\sqrt{3}}{3} \end{bmatrix} \begin{bmatrix} x_A(t) \\ x_B(t) \\ x_C(t) \end{bmatrix} \quad (12)$$

To have a complex rotating component, one can replace the periodic component by a rotating phasor in (6), thus the proposed PCQ-WT is achieved as presented in (13).

$$\vec{\Psi}^{(P)}(t) = \frac{\sqrt{2}}{1 + \cosh(2\pi F_c t)} \cdot e^{j2\pi F_c t} \quad (13)$$

Similar analytics from (9) can be applied to the proposed PCQ-WT, which is

$$\begin{aligned} \vec{X}_{\omega|a,b=0}^{(P)} &= \frac{1}{\sqrt{2a}} \sum_{n=0}^{W/2} \frac{e^{j2\pi(f_0 - \frac{F_c}{a})T_s n}}{(e^{\pi \frac{F_c}{2a} T_s n} + e^{-\pi \frac{F_c}{2a} T_s n})^2 / 4} \\ &= \frac{1}{\sqrt{2a}} \sum_{n=0}^{W/2} \frac{e^{j2\pi(f_0 - \frac{F_c}{a})T_s n}}{\cosh^2(\pi \frac{F_c}{2a} T_s n)} \end{aligned} \quad (14)$$

When  $f_0 = F_c/a$ , the correlation coefficients at the numerator reach their maximum value, i.e., unity. Hence, the complex format of the proposed PCQ-WT focuses on the frequency of interest,  $f_0$ . The following Section will investigate the feature

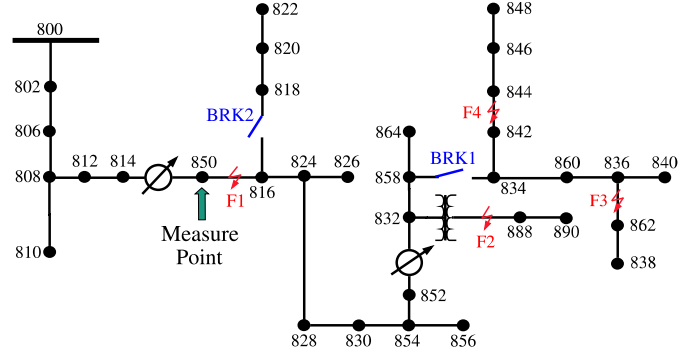


Fig. 5. IEEE 34-Bus test system, with faults and switch locations. The analyzed waveforms are captured at Bus 850.

extraction performance of the proposed wavelets: 1-D PCWT and PCQ-WT.

#### IV. NUMERICAL CASE STUDIES AND WAVEFORM FEATURE EXTRACTION PERFORMANCE EVALUATION

This paper proposed novel wavelet transforms to extract and classify unique features of the input power waveforms and correlate them with various events and grid operating states, in an online setting. In order to evaluate the wavelet performance, the frequency information and patterns extracted from the input waveform are visualized and plotted in the time domain. The evaluation is conducted on the following aspects:

- 1) *Frequency Extraction Sensitivity*: which focuses on examining the frequency resolution of the proposed wavelets where the corresponding pattern appears if there is an off-nominal frequency.
- 2) *Magnitude Sensitivity*: which captures the voltage variation patterns such as voltage swelling and sags.
- 3) *Unbalance Sensitivity*: which focuses on PCQ-WT on three-phase signals during load unbalance or faults.

The following test cases are studied. The time efficiency of the proposed wavelets is evaluated by measuring the time when the event occurs and that when a deformed pattern is detected.

- *Test Case 1*: 5Hz/s frequency ramp.
- *Test Case 2*:  $2^\circ$  phase jump.
- *Test Case 3*: 0.02pu magnitude jump.
- *Test Case 4*: Fault and sudden load change detection.

The IEEE 34-bus test system configuration is illustrated in Fig. 5, where several fault locations are pinpointed in red. Waveforms are captured at Bus 850 and the fault types—single-line-to-ground (SLG), line-line (LL), line-line-to-ground (LLG), and the 3-phase faults—are tabulated in Table I. Each event described in Table I occurred solely at one time, each lasting for 0.2 second.

The frequency response of the PCWT bank which is used for feature extraction in the experiment is shown in Fig. 6, where only 256 scaling factors are utilized to cover up to 3200Hz with sampling rate of  $F_s=9600$ Hz. Note that for PCQ-WT, only the positive range of frequency is valid. Pattern variations indicated in Fig. 7 demonstrate that the *Test Case 1* event is captured within 0.02s and the proposed PCQ-WT could extract a more obvious feature from the waveform than

TABLE I  
DETAILED INFORMATION ON THE SIMULATED FAULTS AND SWITCH  
SETTINGS IN THE IEEE 34-BUS TEST SYSTEM

(a) Fault Data			(b) Switch Settings	
Fault #	Type	Resistance	Breaker #	Initial Status
F1	SLG	0.01 $\Omega$	BRK1	close
F2	LL	0.01 $\Omega$	BRK2	open
F3	LLG	0.01 $\Omega$		
F4	3 $\phi$ G	1 $\Omega$		

\* Only one event occurs at one time interval.

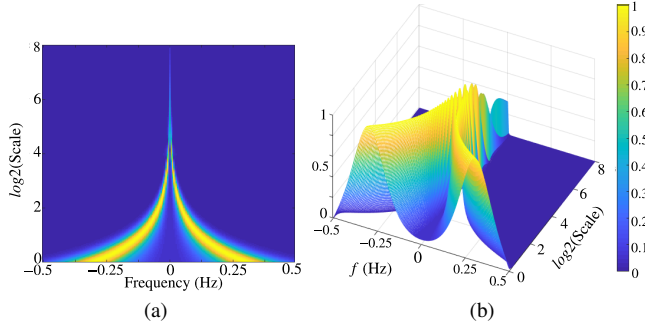


Fig. 6. The impulse response of the PCWT bank in this studied experiment. The frequency and gain is normalized into 1 in X-axis and Z-axis.

the 1-D PCWT. Similar observations can be found in *Test Case 2* and *Test Case 3* in Fig. 8 and Fig. 9: the feature corresponding to a phase and amplitude jump can also be observed within *one cycle* which can be more clearly illustrated through the contours. In *Test Case 2(b)* and *Test Case 3(b)*, the two plots demonstrate that both proposed wavelets can distinguish patterns in different events: distortions in *Test Case 2* is symmetric while being asymmetric in *Test Case 3*.

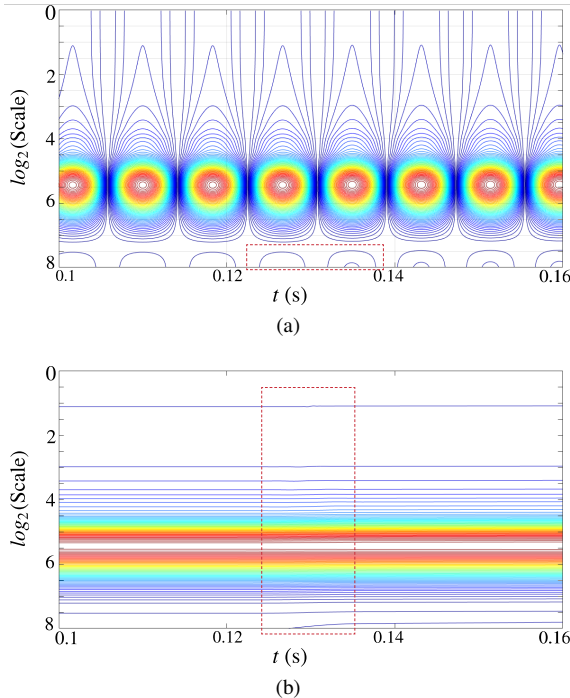


Fig. 7. Simulation results in Test Case 1 where a frequency ramp starts at  $t = 0.12$ s, (a) 1-D PCWT, (b) PCQ-WT.

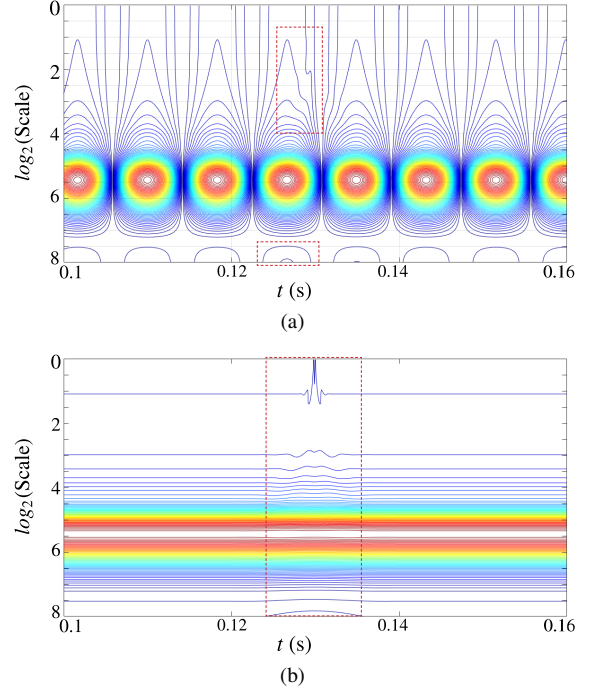


Fig. 8. Simulation results in Test Case 2 where a phase jump occurs at  $t = 0.12$ s, (a) contour of 1-D PCWT, (b) contour of the PCQ-WT.

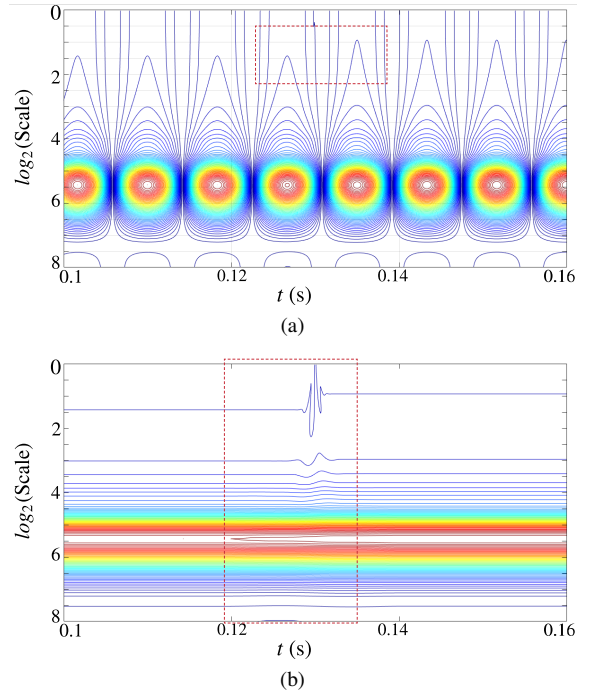


Fig. 9. Simulation results in Test Case 3 where a magnitude jump occurs at  $t = 0.12$ s, (a) contour of 1-D PCWT, (b) contour of the PCQ-WT.

The 1-D PCWT can still capture all the features in the events that are normally hard to be observed. The reason lies in the fact that the 1-D signal amplitude is not fixed over time, thus there are always periodic energy concentrations in 1-D PCWT. One can realize, by comparing the 1-D feature extraction approach in [18], that the proposed 1-D PCWT not only reveals the features around fundamental frequency, but

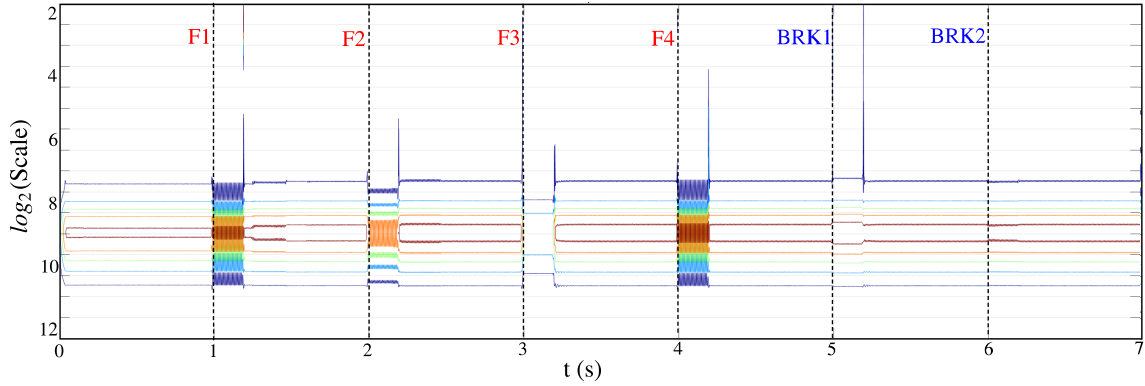


Fig. 10. Contour of the simulation results in Test Case 4 correlated with test events marked.

also those at high frequency range which are associated to the event itself; this would potentially provide more details of the event for the machine learning process to classify the patterns.

In the above dynamic performance tests on pattern extraction mechanism, both the proposed 1-D PCWT and PCQ-WT can extract the features of the events within 20ms, given that the phasor response time limit dictated by the IEEE Std.C37.118.1a-2014 [37] in the presence of amplitude or phase step changes is of two fundamental cycles(33ms). Note that the maximum feature extraction latency (*Test Case 1(a)*) is 17ms. Consequently, the algorithm selection process must be done within 16ms. For compliance, one must ensure that the total time of this process and the remaining time for selecting a suitable algorithm obeys the standard limits.

During the simulated *Test Case 4*, the event analysis demonstrated in Fig. 10 indicates that for different types and locations of faults, the proposed PCQ-WT can successfully detect and extract various features in the system. Since F1 is closer to the measurement point at Bus 850 and F1 is an SLG fault, the feature pattern is observed more obvious than that in the LL and LLG fault scenarios in *Test Case 5*. The proposed PCQ-WT is sensitive to the distance from measurement point and the fault location. The 3-phase fault reveals the highest energy concentration, reflecting a severe impact on the test system. Note that the energy concentration during the normal operating condition is much smaller than that under fault scenarios, thus the extracted feature has much smaller value in the former than that in the latter. This is demonstrated in blue in Fig. 10 at  $t = 0$  to  $t = 1$ . A lost load is also detected at  $t = 5$  and extracted features show that restoration of a small portion of the load is detected at  $t = 6$ . Finally, looking at the entire time span, it can be concluded that the extracted features and patterns are diverse, further highlighting the necessity and promising performance of the proposed wavelet mechanism for online feature extraction.

## V. CONCLUSION

In this paper, new multi-resolution wavelet transforms were introduced for online waveform classification in power systems applications. The waveform classification outcome, if accomplished accurately and computationally-efficient, can be leveraged in PMUs, and other IEDs with PMU functionality,

to select the best synchrophasor estimation algorithm that is most compatible with the system operating condition during which a measurement needs to be captured. The performance of the proposed algorithms, in terms of both feature extraction accuracy and time efficiency, was verified under different test cases representing different operating conditions in the IEEE 34-bus test system. The suggested platform can be embedded in PMUs and help in tracking and capturing the fast and slow variations in the waveform frequency components in both offline and online settings.

## REFERENCES

- [1] E. O. Schweitzer, A. Guzmán, H. J. Altuve, D. A. Tziouvaras, and J. Needs, "Real-time synchrophasor applications in power system control and protection," in *10th IET International Conference on Developments in Power System Protection (DPSP 2010). Managing the Change*, March 2010, pp. 1–5.
- [2] S. Das and T. Sidhu, "A new algorithm to compute fault synchrophasor from transient state synchrophasor in pdc," in *2013 IEEE Power Energy Society General Meeting*, July 2013, pp. 1–5.
- [3] X. Liang and S. A. Wallace, "Processing synchrophasor data using a feature selection procedure," in *2016 IEEE PES Asia-Pacific Power and Energy Engineering Conference (APPEEC)*, Oct 2016, pp. 273–277.
- [4] C. Thilakarathne, L. Meegahapola, and N. Fernando, "Static performance comparison of prominent synchrophasor algorithms," in *2017 IEEE Innovative Smart Grid Technologies - Asia (ISGT-Asia)*, Dec 2017, pp. 1–6.
- [5] S. Wang, P. Dehghanian, and B. Zhang, "A data-driven algorithm for online power grid topology change identification with PMUs," in *2019 IEEE Power Energy Society General Meeting (PESGM)*, Aug 2019, pp. 1–5.
- [6] S. Das and T. Sidhu, "Robust algorithm to estimate fault synchrophasor from fault-transient synchrophasor in phasor data concentrator," *IET Generation, Transmission Distribution*, vol. 9, no. 2, pp. 124–132, 2015.
- [7] "IEEE standard for synchrophasor measurements for power systems," *IEEE Std C37.118.1-2011 (Revision of IEEE Std C37.118-2005)*, pp. 1–61, Dec 2011.
- [8] M. Hossein, R. Koochi, P. Dehghanian, S. Esmaeili, P. Dehghanian, and S. Wang, "A synchrophasor-based decision tree approach for identification of most coherent generating units," in *Annual Conference of the IEEE Industrial Electronics Society*, 2018.
- [9] M. Bertocco, G. Frigo, C. Narduzzi, C. Muscas, and P. A. Pegoraro, "Compressive sensing of a Taylor-Fourier multifrequency model for synchrophasor estimation," *IEEE Transactions on Instrumentation and Measurement*, vol. 64, no. 12, pp. 3274–3283, Dec 2015.
- [10] J. A. de la O Serna and J. Rodríguez-Maldonado, "Taylor-Kalman-Fourier filters for instantaneous oscillating phasor and harmonic estimates," *IEEE Transactions on Instrumentation and Measurement*, vol. 61, no. 4, pp. 941–951, April 2012.

- [11] A. J. Roscoe, I. F. Abdulhadi, and G. M. Burt, "P and M class phasor measurement unit algorithms using adaptive cascaded filters," *IEEE Transactions on Power Delivery*, vol. 28, no. 3, pp. 1447–1459, July 2013.
- [12] P. K. Dash, K. R. Krishnanand, and M. Padhee, "Fast recursive Gauss-Newton adaptive filter for the estimation of power system frequency and harmonics in a noisy environment," *IET Generation, Transmission Distribution*, vol. 5, no. 12, pp. 1277–1289, December 2011.
- [13] A. Z. Amanci and F. P. Dawson, "Synchronization system with zero-crossing peak detection algorithm for power system applications," in *Power Electronics Conference (IPEC), 2010 International*. IEEE, 2010, pp. 2984–2991.
- [14] Á. Ortega and F. Milano, "Comparison of different pll implementations for frequency estimation and control," in *Harmonics and Quality of Power (ICHQP), 2018 18th International Conference on*. IEEE, 2018, pp. 1–6.
- [15] T. Becejac, P. Dehghanian, and M. Kezunovic, "Analysis of PMU algorithm errors during fault transients and out-of-step disturbances," in *IEEE PES Transmission & Distribution Conference and Exposition-Latin America*, 2016, pp. 1–6.
- [16] —, "Probabilistic assessment of PMU integrity for planning of periodic maintenance and testing," in *IEEE International Conference on Probabilistic Methods Applied to Power Systems (PMAPS)*, 2016, pp. 1–6.
- [17] —, "Impact of the errors in the PMU response on synchrophasor-based fault location algorithms," in *2016 North American Power Symposium (NAPS)*, 2016, pp. 1–6.
- [18] C. Qian and M. Kezunovic, "A power waveform classification method for adaptive synchrophasor estimation," *IEEE Transactions on Instrumentation and Measurement*, vol. 67, no. 7, pp. 1646–1658, July 2018.
- [19] F. R. Gomez, A. D. Rajapakse, U. D. Annakkage, and I. T. Fernando, "Support vector machine-based algorithm for post-fault transient stability status prediction using synchronized measurements," *IEEE Transactions on Power Systems*, vol. 26, no. 3, pp. 1474–1483, Aug 2011.
- [20] R. C. Dugan, M. F. McGranaghan, H. W. Beaty, and S. Santoso, *Electrical power systems quality*. mcgraw-Hill New York, 1996, vol. 2.
- [21] S. Wang, P. Dehghanian, M. Alhazmi, J. Su, and B. Shinde, "Resilience-assured protective control of dc/ac inverters under unbalanced and fault scenarios," in *2019 IEEE Power Energy Society Innovative Smart Grid Technologies (ISGT)*, Feb 2019, pp. 1–6.
- [22] S. Khalid and B. Dwivedi, "Power quality issues, problems, standards & their effects in industry with corrective means," *International Journal of Advances in Engineering & Technology*, vol. 1, no. 2, p. 1, 2011.
- [23] F. A. S. Borges, R. A. S. Fernandes, I. N. Silva, and C. B. S. Silva, "Feature extraction and power quality disturbances classification using smart meters signals," *IEEE Transactions on Industrial Informatics*, vol. 12, no. 2, pp. 824–833, April 2016.
- [24] M. S. Manikandan, S. R. Samantaray, and I. Kamwa, "Detection and classification of power quality disturbances using sparse signal decomposition on hybrid dictionaries," *IEEE Transactions on Instrumentation and Measurement*, vol. 64, no. 1, pp. 27–38, Jan 2015.
- [25] K. Thirumala, M. S. Prasad, T. Jain, and A. C. Umarikar, "Tunable-q wavelet transform and dual multiclass svm for online automatic detection of power quality disturbances," *IEEE Transactions on Smart Grid*, vol. 9, no. 4, pp. 3018–3028, July 2018.
- [26] M. H. R. Koochi, P. Dehghanian, S. Esmaili, P. Dehghanian, and S. Wang, "A synchrophasor-based decision tree approach for identification of most coherent generating units," in *IECON 2018 - 44th Annual Conference of the IEEE Industrial Electronics Society*, Oct 2018, pp. 71–76.
- [27] D. P. Mishra, S. R. Samantaray, and G. Joos, "A combined wavelet and data-mining based intelligent protection scheme for microgrid," *IEEE Transactions on Smart Grid*, vol. 7, no. 5, pp. 2295–2304, Sept 2016.
- [28] P. Rajaraman, N. A. Sundaravaradan, R. Meyur, M. J. B. Reddy, and D. K. Mohanta, "Fault classification in transmission lines using wavelet multiresolution analysis," *IEEE Potentials*, vol. 35, no. 1, pp. 38–44, Jan 2016.
- [29] C. Torrence and G. P. Compo, "A practical guide to wavelet analysis," *Bulletin of the American Meteorological society*, vol. 79, no. 1, pp. 61–78, 1998.
- [30] P. S. Addison, *The illustrated wavelet transform handbook: introductory theory and applications in science, engineering, medicine and finance*. CRC press, 2017.
- [31] M. Stephane, *A wavelet tour of signal processing*. Elsevier, 1999.
- [32] S. Mallat and W. L. Hwang, "Singularity detection and processing with wavelets," *IEEE Transactions on Information Theory*, vol. 38, no. 2, pp. 617–643, March 1992.
- [33] J. R. Williams and K. Amaratunga, "A discrete wavelet transform without edge effects using wavelet extrapolation," *Journal of Fourier Analysis and Applications*, vol. 3, no. 4, pp. 435–449, 1997.
- [34] B. Tang, T. Song, F. Li, and L. Deng, "Fault diagnosis for a wind turbine transmission system based on manifold learning and shannon wavelet support vector machine," *Renewable Energy*, vol. 62, pp. 1–9, 2014.
- [35] C. Cattani, "Shannon wavelets theory," *Mathematical Problems in Engineering*, vol. 2008, 2008.
- [36] W. Dueterhoeft, M. W. Schulz, and E. Clarke, "Determination of instantaneous currents and voltages by means of alpha, beta, and zero components," *Transactions of the American Institute of Electrical Engineers*, vol. 2, no. 70, pp. 1248–1255, 1951.
- [37] "IEEE standard for synchrophasor measurements for power systems – amendment 1: Modification of selected performance requirements," *IEEE Std C37.118.1a-2014 (Amendment to IEEE Std C37.118.1-2011)*, pp. 1–25, April 2014.